Ultrahigh-sensitivity temperature fiber sensor based on multimode interference

Susana Silva,[1,2,3] Edwin G. P. Pachon,[1] Marcos A. R. Franco,[4] Juliano G. Hayashi,[1] F. Xavier Malcata,[5,6] Orlando Frazão,[3] Pedro Jorge,[3] and Cristiano M. B. Cordeiro[1]

[1]Instituto de Física "Gleb Wataghin," Universidade Estadual de Campinas–UNICAMP, Campinas, São Paulo, Brazil

[2]Departamento de Física e Astronomia, Faculdade de Ciências da Universidade do Porto, Rua do Campo Alegre 687, 4169-007 Porto, Portugal

[3]INESC-Porto, Rua do Campo Alegre 687, 4169-007 Porto, Portugal

[4]Instituto de Estudos Avançados, São José dos Campos, São Paulo, Brazil

[5]ISMAI–Instituto Superior da Maia, Avenida Carlos Oliveira Campos, 4475-690 Avioso São Pedro, Portugal

[6]Instituto de Tecnologia Química e Biológica, Universidade Nova de Lisboa, Avenida da República, 2780-157 Oeiras, Portugal

*Corresponding author: sfsilva@inescporto.pt

Received 5 December 2011; revised 6 February 2012; accepted 8 February 2012; posted 8 February 2012 (Doc. ID 159363); published 23 May 2012

The proposed sensing device relies on the self-imaging effect that occurs in a pure silica multimode fiber (coreless MMF) section of a single-mode–multimode–single-mode (SMS)-based fiber structure. The influence of the coreless-MMF diameter on the external refractive index (RI) variation permitted the sensing head with the lowest MMF diameter (i.e., 55 μm) to exhibit the maximum sensitivity (2800 nm/RIU). This approach also implied an ultrahigh sensitivity of this fiber device to temperature variations in the liquid RI of 1.43: a maximum sensitivity of −1880 pm/°C was indeed attained. Therefore, the results produced were over 100-fold those of the typical value of approximately 13 pm/°C achieved in air using a similar device. Numerical analysis of an evanescent wave absorption sensor was performed, in order to extend the range of liquids with a detectable RI to above 1.43. The suggested model is an SMS fiber device where a polymer coating, with an RI as low as 1.3, is deposited over the coreless MMF; numerical results are presented pertaining to several polymer thicknesses in terms of external RI variation.

OCIS codes: 060.0060, 060.2310, 060.2370, 120.6780.

1. Introduction

Multimode interference (MMI) on optical fiber devices has been thoroughly investigated as an attractive technology for optical communication and sensing [1]. A typical example is the single-mode–multimode–single-mode (SMS) fiber structure—which, owing to its unique spectral characteristics, has found many applications, e.g., in edge filtering for wavelength measurement [2], refractometry [3], strain measurement with compensation of temperature [4], and curvature sensing [5].

The self-imaging phenomenon in waveguided devices is a well-known concept [6]; in recent years, many efforts have been made to develop MMI-based fiber devices based on such a concept. Mohammed *et al.* [7] reported a fiber structure relying on the self-imaging effect for bandpass filtering; in this case, the sensing head was a section of a pure silica multimode fiber (coreless MMF)—125 μm in diameter and 57.7 mm in length, spliced between two single-mode

1559-128X/12/163236-07$15.00/0

fibers (SMFs), and proposed as a fixed-wavelength bandpass filter. The wavelength peak arising from the self-image could be adjusted by changing the MMF length, or finely tuned via application of strain on the fiber device. Later, Antonio-Lopez *et al.* [8] developed an SMS fiber-based wavelength-tunable filter; the total MMF section relied on two spliced sections of a standard MMF with 105/125 μm core and cladding diameters, respectively, and coreless MMF with 125 μm diameter, so that the combined length still formed a self-image at the end of the MMF. A capillary tube filled with refractive-index-matching liquid was used between the 105/125 μm MMF section and the input SMF, to effectively increase the length of the total MMF section—and accordingly achieve wavelength tuning.

A different approach relied on a fiber tip sensor for liquid level measurement [9]. The sensing structure was a 125 μm diameter coreless-MMF section spliced to an SMF, with 60.816 mm in length corresponding to a self-image plane; the MMF tip was coated with a 200 nm thick layer of gold acting as mirror, so that the self-image was backreflected and coupled into the SMF. Therefore, when the coreless MMF was immersed in a liquid and its level was changed, a correlated shift of the wavelength peak was found. Wu *et al.* [10] produced, in turn, a displacement sensor based on a bent SMS fiber structure. A standard 105/125 μm MMF section was consequently used, with a length of 42.1 mm to ensure self-imaging. The bending decreased the risk of fiber breakage, as well as the limitation of displacement range that typically occurs in a straight fiber device.

Recently, another SMS fiber-based refractometer relying on the self-imaging concept was reported [11]; a chemically etched core MMF was used, with different diameters and lengths tested, in attempts to unfold its influence on the sensitivity to refractive index (RI) measurement. Within the RI range (1.345–1.43), fiber devices having etched core MMFs with diameters of 50, 80, and 105 μm were analyzed; numerical results have shown that the sensitivity to external RI increased when the etched MMF core diameter decreased. However, experimental validation was performed only with etched core MMFs with 80 and 105 μm in diameter. On the other hand, Aguilar-Soto *et al.* [12] used the self-imaging effect of an SMS fiber structure, based on a coreless MMF with 125 μm in diameter, to measure temperature; a typical sensitivity of approximately 13 pm/°C in the temperature range from 25°C to 375°C was achieved.

This work conveys experimental results based on the MMI concept—which was intended here to measure RI variations of the surrounding medium, in order to ascertain the temperature dependence in a high-sensitivity RI range. The proposed sensing device is based on an SMS fiber structure in which a section of coreless MMF was used. Three MMFs with different diameters were tested, namely, 55, 78, and 125 μm; and the influence of diameter upon the sensitivity to RI variations was ascertained. Both numerical simulations and experimental results showed that the sensitivity to RI would increase if the coreless-MMF diameter decreased; a maximum sensitivity of 2800 nm/RIU was indeed attained for the sensing head with a coreless MMF of 55 μm in diameter. Therefore, our fiber device has shown to be highly sensitive to temperature variations for a liquid RI of 1.43 (i.e., a nominal value of 1.44)—and a maximum sensitivity of −1880 pm/°C was attained. The beam-propagation method (BPM) was employed in modeling light propagation along the proposed fiber structure—and a comparison between experimental data and numerical simulations is presented.

2. Results

The proposed sensing head consists of a coreless-MMF section, spliced between two SMFs and interrogated in transmission; this is schematically shown in Fig. 1. The coreless MMF is a pure silica rod characterized by a RI of 1.444. A broadband source (BBS) in the 1550 nm spectral range was employed—with a bandwidth of 300 nm and an optical spectrum analyzer (OSA) as the interrogation unit.

The theoretical basis underlying the SMS-based fiber structure concept is that when the light field propagating along the input SMF enters the MMF section, several modes of the MMF are excited; hence, differential phases between the modes will accumulate, while the light beam propagates along the remainder of the MMF section. Although the global field profile changes along the MMF section, it

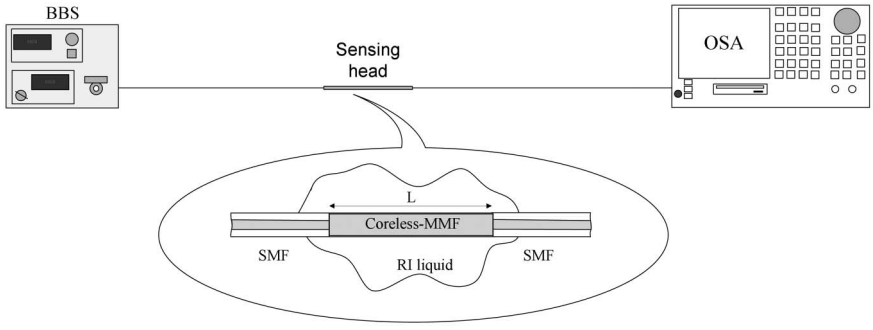

Fig. 1. Experimental setup utilized and detail of the coreless-MMF-based SMS fiber structure.

remains symmetrically distributed along the direction of propagation [13]. Therefore, distinct propagation distances correspond to different field profiles at the exit end of an MMF with a given length L. Furthermore, there are several fractional planes where field condensation occurs—some of which are periodic planes where self-imaging takes place [14,15]. The self-imaging distance (Z_i) thus pertains to where the light field at the input of the MMF section is replicated, in both amplitude and phase, on the output of the MMF for a specific wavelength; hence, it can be calculated as

$$Z_i = \frac{4D^2 n_{\text{core}}}{\lambda}, \tag{1}$$

where D and n_{core} are the MMF diameter and core RI, respectively, and λ is the operational wavelength. In this specific case, the light field condensation in a particular plane results from constructive interference between the several guided modes; whereas in the case of the fractional (not self-imaging) planes, one may assume constructive interference between two consecutive modes that were excited with the highest coupling efficiency. It should be noted that only the first self-image (and multiples) will exhibit minimum losses, and those will be used during this work.

The operating mechanism of our sensing head relies on the self-imaging phenomenon that occurs for a specific length of the coreless MMF used, thus providing a well-defined wavelength peak—which in principle will be sensitive to the cladding (a role played here by the liquid) RI variations. Considering that the thermo-optic coefficient of water is approximately 10^{-4} K^{-1} [16], higher sensitivities to liquid RI are expected than if RI variations were measured in air—where the thermo-optic effect is lower, approximately 10^{-6} K^{-1} [17]. As shown below, the proposed fiber device will be suitable for high-sensitivity measurement of temperature for a liquid RI of 1.43 (i.e., a nominal value of 1.44).

To further develop this study, a three-dimensional simulation based on the BPM [18] was taken advantage of to investigate the beam behavior in the coreless-MMF section of an SMS fiber structure in transmission, relying on the self-imaging effect and when submitted to different external RIs. To investigate the influence of the coreless-MMF diameter in the presence of external RI variation, the first self-image length was selected for both numerical and experimental analysis.

The modeling of light propagation was done for a pure silica fiber with a RI of 1.444 and three different diameters, namely, 55, 80, and 125 μm. SMFs with core and cladding diameters of 8.2 and 125 μm, respectively, were used for both light input and output of the coreless-MMF section. All fibers were aligned along the same axis and possessed a circular cross section. Our numerical simulations have shown that the optimized MMF length was 11.5, 24.2, and 58.9 mm, for the fiber structures with coreless-MMF diameters of 55, 80, and 125 μm, respectively. The intensity distribution of the electric field on the xz plane at the simulated coreless-MMF length of 11.5 mm and diameter of 55 μm is plotted in Figs. 2(a)–2(d)—when exposed to external RI of 1.0, 1.3, 1.36, and 1.42, respectively, and for operation at a fixed wavelength of 1550 nm.

Inspection of Fig. 2(a) shows clearly that, when the light field coming from the input SMF enters the coreless MMF at $z = 0$ mm, interference between the different modes occurs along the MMF section (z direction). One further notices enhanced fractional planes where the light field appears to concentrate along the coreless-MMF section—located at approximately 2.5, 9, and 11.5 mm; however, the first self-image is located at its exit end, $Z_i = 11.5$ mm (modeling was extended until 12.5 mm, for better visualization), thus exhibiting minimum losses. Here, the whole light field condensates into one point, due

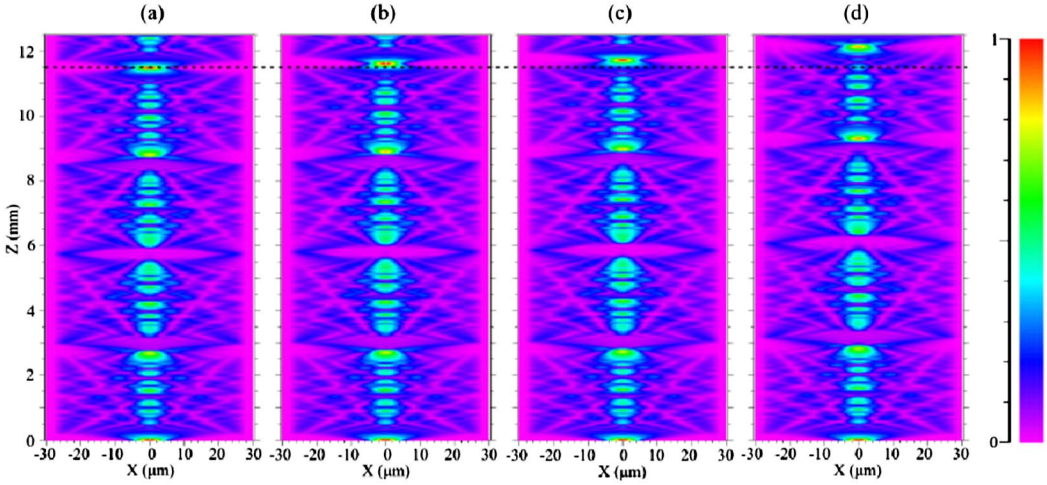

Fig. 2. (Color online) Intensity distribution on the x–z plane of the electric field at the 1550 nm wavelength for the SMS fiber structure with a coreless-MMF diameter of 55 μm, when exposed to external the RI of (a) 1.0, (b) 1.3, (c) 1.36, and (d) 1.42.

to constructive interference between the several modes—to be recoupled into the output SMF. When the RI of the surrounding medium took higher values [see Figs. 2(b)–2(d)], the self-image plane moved forward to higher lengths of the coreless-MMF section. In the situation of a broadband optical field (Fig. 1), this corresponds to a spectral wavelength peak of the sensing structure to shift as well.

Three coreless MMFs with different diameters, namely, 55, 78, and 125 μm (SMS_1, SMS_2, and SMS_3, respectively), were experimentally tested. Splices between the coreless MMF and SMFs were performed manually with a fiber fusion splicing machine (FITEL S177A). Because of MMFs with smaller diameters than the SMF, perfect alignment in the splicing process could not be guaranteed; a maximum misalignment of approximately 5 μm for SMS_1 was estimated. The length of each coreless-MMF section was set so as to provide a well-defined wavelength peak in the operational wavelength range of 1400–1700 nm. A digital caliper and a fiber-cutting machine were used to measure and cut each MMF section with the desired length (to an upper measurement error of 0.5 mm), respectively. The fiber devices were analyzed by optical microscopy, and the optimized length able to achieve the first self-imaging point was 11.45, 21.37, and 58.23 mm, for SMS_1, SMS_2, and SMS_3, respectively. These values are in good agreement with those obtained by numerical simulation and based on Eq. (1) with $n_{core} = 1.444$ and $\lambda = 1550$ nm.

The response of each structure to external RI variations was evaluated in detail. The sensing device characterization was performed by exposing each sensing head to liquids bearing distinct RIs in the range 1.30–1.43. A series of commercial RI standards from Cargille Laboratories (Cedar Grove, N.J.) were accordingly used; such standards were properly corrected for the operational wavelength of 1550 nm and room temperature (20°C). The optical spectra of SMS_1, SMS_2, and SMS_3 for three different external RI (i.e., 1, 1.33, and 1.4) are depicted in Fig. 3.

Each sensing structure has a wavelength peak used for RI measurements, with a full-width at half-maximum (FWHM) of approximately 48, 33, and 11 nm, for SMS_1, SMS_2, and SMS_3, respectively. Results have shown that the device exhibited a substantial change in amplitude of the optical signal, as a consequence of the change in the reflection coefficient at the coreless MMF/liquid interface. The amplitude of the optical signal decreased, due to the increase of the surrounding liquid RI while approaching the silica RI of the coreless MMF. Furthermore, a wavelength shift occurred because the effective RI of the guided modes at the coreless MMF changed when the sensing structure was submitted to RI variations of the external medium. The wavelength dependence of each sensing head on the RI variation of the surrounding medium is shown in Fig. 4, in agreement with the result obtained with an etched core MMF fiber [11].

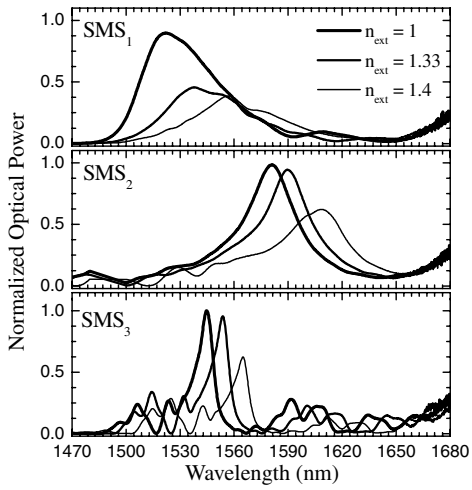

Fig. 3. Experimental spectral response of the SMS fiber structures with different coreless-MMF diameters, namely, 55, 78, and 125 μm (SMS_1, SMS_2, and SMS_3, respectively), to distinct RIs, namely, 1, 1.33, and 1.4.

According to Fig. 4, the numerical simulations are in good agreement with the experimental results generated. As anticipated, the wavelength shift increases with increasing liquid RI but the behavior is not linear within the RI range studied. Analysis of the simulated results [Fig. 4(a)] showed that, in the lower RI range (1.30–1.33), estimated sensitivities of 186, 134, and 104 nm/RIU, for SMS_1,

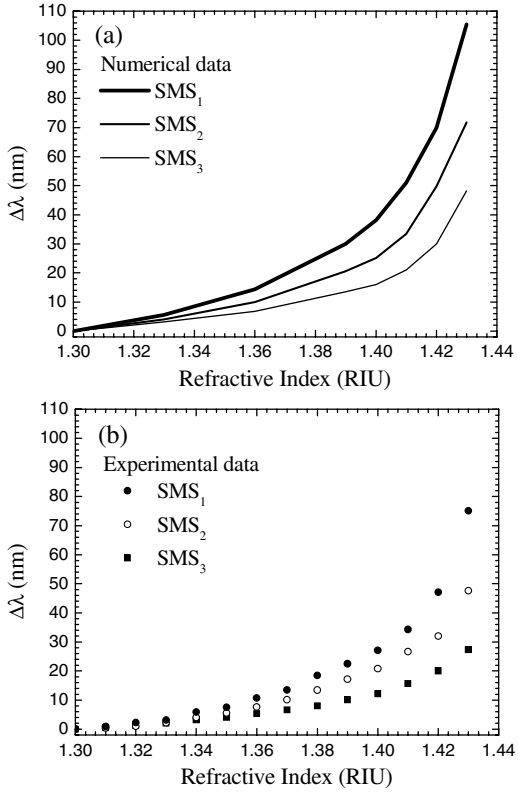

Fig. 4. Wavelength shift of fiber structures SMS_1, SMS_2, and SMS_3 in response to RI variations as (a) numerical data and (b) experimental results.

Table 1. Sensitivity Coefficients for the Refractive Index

	Refractive Index (nm/RIU)			
	RI Range 1.30–1.33		RI Range 1.42–1.43	
	Numerical	Experimental	Numerical	Experimental
SMS_1	186	140	3550	2800
SMS_2	134	98	2190	1560
SMS_3	104	79	1820	735

SMS_2, and SMS_3, respectively, could be achieved; conversely, in the high-sensitivity RI region (1.42–1.43), much higher typical values of 3550, 2190, and 1820 nm/RIU, for SMS_1, SMS_2, and SMS_3, respectively, were attained. The fiber structure SMS_1 is more sensitive to RI variations due to its smaller coreless-MMF diameter, because the interaction between the interfered high-order modes and the external medium is increased. In the lower RI range (1.30–1.33), sensitivities of 140, 98, and 79 nm/RIU, for SMS_1, SMS_2, and SMS_3, respectively, were observed [Fig. 4(b)], whereas in the upper RI range (1.42–1.43), typical values of 2800, 1560, and 735 nm/RIU, for SMS_1, SMS_2, and SMS_3, respectively, were achieved instead. These results are summarized in Table 1.

A previous study using the MMI of a large-core air-clad photonic crystal fiber-based sensing structure has unfolded the influence of temperature upon the RI response using water as the test fluid—and a maximum sensitivity of 800 nm/RIU was observed [19]. Using this feature, the proposed fiber device appears suitable to measure the temperature, with an enhanced sensitivity for a liquid RI of 1.43. To perform this experiment, the sensing head with the coreless-MMF diameter of 55 μm (SMS_1) was used to ensure maximum sensitivity. The sensing device was placed in contact with a Cargille RI liquid, with a nominal value of 1.44, to measure temperature variations in the high-sensitivity RI range, namely, 1.42–1.43. At the operational wavelength of 1550 nm and room temperature (20°C), the nominal value 1.44 is to be corrected to 1.4298—considering a thermo-optic coefficient of -3.95×10^{-4}. The fiber structure was submitted to increasing values of temperature (ΔT) in the range [0°C–80°C], at 5°C steps—and the corresponding results are depicted in Fig. 5.

Inspection of Fig. 5 indicates that the sensing head produces a nonlinear response to temperature variations—characterized by an ultrahigh sensitivity of −1880 pm/°C in the temperature range 0°C–25°C. These results are over 100-fold the typical value of approximately 13 pm/°C achieved in air with a similar fiber structure [12]. From 25°C to 80°C, a sensitivity of −360 pm/°C was recorded.

In practice, a temperature change induces coreless-MMF length variation (due to thermal expansion) and RI variation of the coreless MMF (due to silica thermo-optic effect); hence, an optical path length variation occurs, with an associated wavelength scaling for the measured region. Using a surrounding liquid with the proper RI, a high sensitivity to temperature may thus be obtained—with the possibility to choose the temperature range to be measured only by rescaling the external medium RI. The bottom line is that when temperature increases the RI of the liquid decreases and sensitivity to temperature decreases as well.

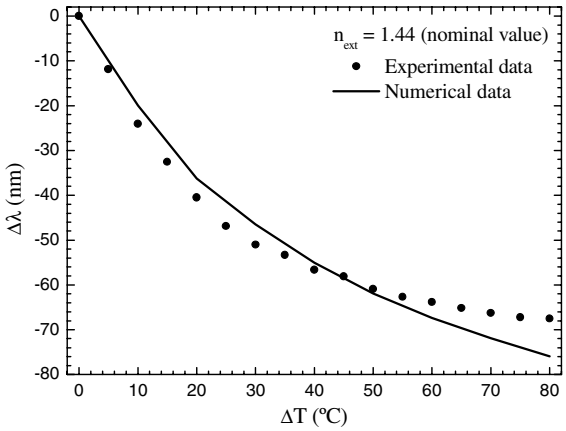

Fig. 5. Wavelength shift of sensing structure SMS_1 to temperature variation, in the high-sensitivity RI range (1.42–1.43) using a liquid RI with a nominal value of 1.44 (20°C), as numerical data and experimental results.

For instance, sensitivity as low as 188 pm/°C is obtained when a liquid with nominal RI of 1.44 is used, suitable to measure temperature in the 60°C–80°C range. Rescaling the liquid RI to a nominal value of, say, 1.46 at 20°C, would lead to a high sensitivity but in the temperature range of 60°C–80°C. The numerical simulation unfolds a pattern similar to experimental evidence (see Fig. 5). In this case, the RI variation of the fiber due to the silica thermo-optic effect was taken into account; the effect of thermal expansion over the MMF length variation was not taken into account, because it is much smaller than the thermo-optic effect.

Although showing a high sensitivity to RI variations, the proposed SMS fiber structure is always restricted to external RI values below the effective RI of the guided modes. Numerical analysis of an evanescent wave absorption sensor was performed in attempts to overcome this limitation. The suggested model is an SMS fiber device where a polymer coating, with an RI as low as 1.3, is deposited over the coreless-MMF section—aimed at extending the range of possible liquid RI values around the MMF to above 1.43. Note that the proposed sensing concept for the measurement of external RI changes is based on evanescent wave absorption induced by the measurand. Numerical simulations were then performed for the sensing head characterized by a coreless-MMF diameter of 125 μm and coated with a polymer layer of varying thickness, namely, 0.5, 0.75, 1.0, and 1.5 μm. The results obtained are available as Fig. 6(a).

Numerical results indicates that a polymer thickness of 1.0 or 1.5 μm leads to a poor change

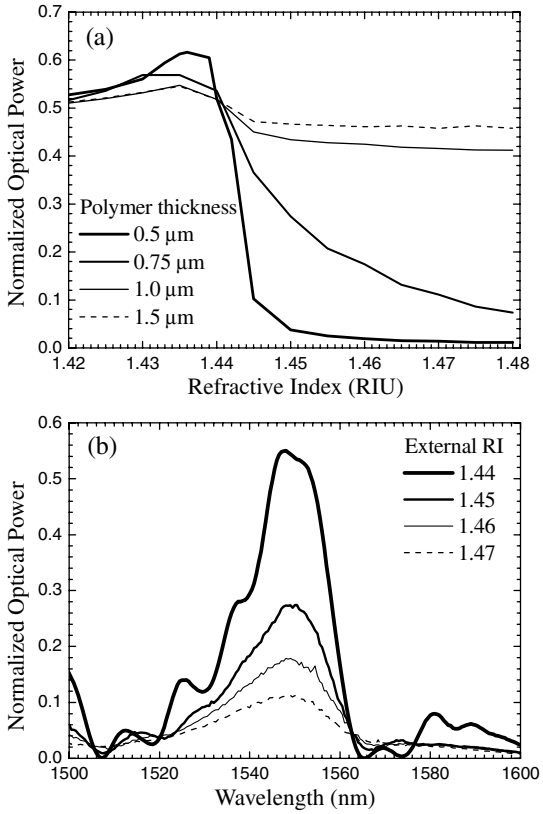

Fig. 6. (a) Intensity variation of SMS fiber structure with coreless-MMF diameter of 125 μm, and coated with 0.5, 0.75, 1, and 1.5 μm thick polymer layers, when submitted to external RI in the range (1.42–1.48) and (b) spectral changes of SMS fiber structure with coreless-MMF diameter of 125 μm, and coated with a 0.75 μm thick polymer layer, when submitted to external RI in the range (1.44–1.47).

in intensity, approximately 0.14 and 0.1, respectively; conversely, for a polymer thickness of 0.5 and 0.75 μm, the intensity change is higher, approximately 0.6 and 0.5, respectively. On the other hand, one observes a decrease of the signal to nearly zero after 1.45 RIU, for polymer thicknesses of 0.5, 1.0, and 1.5 μm, thus leading to an effective measurable RI range from 1.435 to 1.45. This means that, for insufficient polymer thickness, the evanescent wave escapes into the surrounding medium that acts as cladding, whereas for an excessive film thickness, the evanescent wave absorption is weak, and thus it is less sensitive to the surrounding medium. Therefore, the optimized polymer thickness found is 0.75 μm as it couples a high intensity change to an effective measurable RI range (1.43–1.48).

The proposed sensing device appears suitable for measurement of an external RI above 1.43, via intensity variations of the signal [as shown in Fig. 6(b)]. In the past, a pH sensor based on a plastic cladding silica fiber coated with multiple sol-gel layers was previously proposed [20]—and the sensing principle used was intensity variations of the signal via evanescent wave absorption in the sensing region of the fiber structure. The optimum thickness of the thin film was found to be approximately 0.6 μm—which is consistent with our numerical results.

3. Conclusions

This paper reports on a highly sensitive temperature sensor, based on MMI. The sensing concept relies on the self-imaging effect that occurs in a coreless-MMF-based SMS fiber structure interrogated in transmission, and it is intended to measure RI variations of a surrounding medium in order to ascertain the temperature dependence in a high-sensitivity RI range.

Three MMFs with different diameters, namely, 55, 78, and 125 μm, were used, and the influence of diameter upon the sensitivity to RI variations was assessed in the range of (1.3–1.43). The sensitivity to external RI variations increased when the coreless-MMF diameter was decreased; a maximum sensitivity of 2800 nm/RIU for the SMS fiber structure with the lowest coreless-MMF diameter (55 μm) was achieved. This sensing device thus proved to be highly sensitive to temperature variations in the liquid RI of 1.43 (with a nominal value 1.44)—with the maximum sensitivity of −1880 pm/°C. Our results are more than 100-fold typical values, approximately 13 pm/°C and 10 pm/°C, achieved in air with a coreless-MMF-based SMS fiber structure and an FBG, respectively.

The BPM was employed in modeling light propagation along the SMS fiber structure, for the sake of comparison of experimental data to numerical simulations; a good agreement was found between them. The proposed fiber device has a high potential for measurement of RI and temperature—although restricted to external RI values below the effective RI of the guided modes. To overcome this drawback, numerical analysis of an evanescent wave absorption sensor was performed. The model suggested was based on an SMS fiber structure, in which a coreless MMF with diameter of 125 μm was coated with a polymer layer, and an RI as low as 1.3 was tested with the purpose of extending the range of possible RI liquids around the MMF fiber to above 1.43. Numerical simulations indicated that the optimized polymer thickness is 0.75 μm for an RI range of (1.42–1.48).

Therefore, the proposed sensing device appears suitable for a variety of applications in food and oil research—either by changing the diameter of the coreless MMF or coating it with a polymer layer; it will likely display a high sensitivity to external RI or temperature, along an extended RI range, say (1.30–1.48).

This work was partially supported by a binational collaboration project between the Coordenação de Aperfeiçoamento de Pessoal de Nível Superior (CAPES) and the Fundação para a Ciência e Tecnologia (FCT) CAPES-FCT Brazil/Portugal (# 293/11, coordinated by authors C. M. B. C. and P. J.), by the Financiadora de Estudos e Projetos (FINEP), by project Pró-Defesa CAPES/Ministério da Defesa

(ref. 23038.029912/2008-05), and by project MICROPHYTE (ref. PTDC/EBB-EBI/102728/2008), funded by the European Union (EU) and the Portuguese State and coordinated by author F. X. M., as well as project COST 299, funded by the EU. Author S. S. received a Ph.D. fellowship (ref. SFRH/BD/47799/2008), also funded by the EU and the Portuguese State and supervised by author F. X. M.

References

1. A. Kumar, R. K. Varshney, C. S. Antony, and P. Sharma, "Transmission characteristics of SMS fiber optic sensor structures," Opt. Commun. **219**, 215–219 (2003).
2. Q. Wang and G. Farrell, "Multimode-fiber-based edge filter for optical wavelength measurement application," Microw. Opt. Technol. Lett. **48**, 900–902 (2006).
3. P. Wang, G. Brambilla, M. Ding, Y. Semenova, Q. Wu, and G. Farrell, "High-sensitivity, evanescent field refractometric sensor based on a tapered, multimode fiber interference," Opt. Lett. **36**, 2233–2235 (2011).
4. A. M. Hatta, Y. Semenova, Q. Wu, and G. Farrell, "Strain sensor based on a pair of single-mode-multimode-single-mode fiber structures in a ratiometric power measurement scheme," Appl. Opt. **49**, 536–541 (2010).
5. S. Silva, O. Frazão, J. Viegas, L. A. Ferreira, F. M. Araújo, F. X. Malcata, and J. L. Santos, "Temperature and strain-independent curvature sensor based on a singlemode/multimode fiber optic structure," Meas. Sci. Technol. **22**, 085201 (2011).
6. L. B. Soldano and E. C. M. Pennings, "Optical multi-mode interference devices based on self-imaging: principles and applications," J. Lightwave Technol. **13**, 615–627 (1995).
7. W. S. Mohammed, P. W. E. Smith, and X. Gu, "All-fiber multimode interference bandpass filter," Opt. Lett. **31**, 2547–2549 (2006).
8. J. E. Antonio-Lopez, A. Castillo-Guzman, D. A. May-Arrioja, R. Selvas-Aguilar, and P. L. Wa, "Tunable multimode-interference bandpass fiber filter," Opt. Lett. **35**, 324–326 (2010).
9. J. E. Antonio-Lopez, J. J. Sanchez-Mondragon, P. L. Wa, and D. A. May-Arrioja, "Fiber-optic sensor for liquid level measurement," Opt. Lett. **36**, 3425–3427 (2011).
10. Q. Wu, Y. Semenova, P. Wang, A. M. Hatta, and G. Farrell, "Experimental demonstration of a simple displacement sensor based on a bent single-mode–multimode–single-mode fiber structure," Meas. Sci. Technol. **22**, 025203 (2011).
11. Q. Wu, Y. Semenova, P. Wang, and G. Farrell, "High sensitivity SMS fiber structure based refractometer—analysis and experiment," Opt. Express **19**, 7937–7944 (2011).
12. J. G. Aguilar-Soto, J. E. Antonio-Lopez, J. J. Sanchez-Mondragon, and D. A. May-Arrioja, "Fiber optic temperature sensor based on multimode interference effects," J. Phys. **274**, 012011 (2011).
13. Q. Wang, G. Farrell, and W. Yan, "Investigation on single-mode-multimode-singlemode fiber structure," J. Lightwave Technol. **26**, 512–519 (2008).
14. W. S. Mohammed, P. W. E. Smith, and X. Gu, "Wavelength tunable fiber lens based on multimode interference," J. Lightwave Technol. **22**, 469–477 (2004).
15. A. Mehta, W. Mohammed, and E. G. Johnson, "Multimode interference-based fiber-optic displacement sensor," IEEE Photon. Technol. Lett. **15**, 1129–1131 (2003).
16. G. Abbate, U. Bernini, E. Ragozzino, and F. Somma, "The temperature dependence of the refractive index of water," J. Phys. D **11**, 1167–1172 (1978).
17. J. C. Owens, "Optical refractive index of air: dependence on pressure, temperature and composition," Appl. Opt. **6**, 51–59 (1967).
18. K. Kawano and T. Kitoh, *Introduction to Optical Waveguide Analysis* (Wiley, 2001), Chap. 5, pp. 165–230.
19. S. Silva, J. L. Santos, F. X. Malcata, J. Kobelke, K. Schuster, and O. Frazão, "Optical refractometer based on large-core, air-clad photonic crystal fibers," Opt. Lett. **36**, 852–854, (2011).
20. S. T. Lee, J. Gin, V. P. N. Nampoori, C. P. G. Vallabhan, N. V. Unnikrishnan, and P. Radhakrishnan, "A sensitive fibre optic pH sensor using multiple sol-gel coatings," J. Opt. A **3**, 355–359 (2001).